Structural and kinetic study of phase transitions in $La_{2-x}Y_xSi_2O_7$ (x=1.0). Mechanical properties of the high temperature polymorph.

Alberto José Fernández-Carrión,[1] Alberto Escudero[1] Matthew Suchomel[2] and Ana Isabel Becerro[1]*

[1]Instituto de Ciência de Materiales de Sevilla (CSIC-Universidad de Sevilla). c/ Américo Vespucio, 49. 41092 Seville (Spain). Departamento de Química Inorgánica (Universidad de Sevilla), c/Profesor García-González, 1, 41071 Sevilla, Spain

[2]Advanced Photon Source, Argonne National Laboratory, Argonne, IL 60439 (USA)

Abstract

Phase transitions in $La_{1.0}Y_{1.0}Si_2O_7$ have been studied as a function of temperature using XRD and TEM. In agreement with the "radius criterion" $La_{1.0}Y_{1.0}Si_2O_7$ solid solution should crystallize as tetragonal A- $La_{1.0}Y_{1.0}Si_2O_7$ phase at temperatures below ~1500ºC. However, although A- $La_{1.0}Y_{1.0}Si_2O_7$ can be obtained after calcination at 1100 ºC and 1200 ºC for 1 day, it transforms in the monoclinic G-$La_{1.0}Y_{1.0}Si_2O_7$ phase when calcination time is increased. Therefore, A- $La_{1.0}Y_{1.0}Si_2O_7$ is not a thermodynamically stable phase and the "radius criterion" is not obeyed in this silicate system. The A→ G phase transition is extremely sluggish. It needs ca. 250 hours to be completed at 1200ºC, while complete transformation was not observed after 21 days calcination at 1100 ºC. Finally, transformation of G- into F-$La_{1.0}Y_{1.0}Si_2O_7$ was not observed in this composition. The structural study of both phases by laboratory and synchrotron XRD and TEM/EDX indicates that Y enters the La sites in both A- and G- $La_{1.0}Y_{1.0}Si_2O_7$ unit cells forming solid solutions of both polymorphs. In G- $La_{1.0}Y_{1.0}Si_2O_7$, La occupies preferentially the rare earth crystallographic site 1 while Y is located in the rare earth site 2. The incorporation of Y in the G-$La_2Si_2O_7$ structure creates a high degree of local disorder around the Si atoms, as inferred from ^{29}Si MAS NMR spectroscopy measurements. Finally, G-$La_{1.0}Y_{1.0}Si_2O_7$ shows a high fracture toughness value that suggests that G-$La_{1.0}Y_{1.0}Si_2O_7$ could be a good damage-tolerant ceramic.

* Corresponding author. e-mail address: anieto@icmse.csic.es

Keywords: yttrium disilicate, lanthanum disilicate, $Y_2Si_2O_7$, $La_2Si_2O_7$, ^{29}Si MAS NMR, Rietveld refinement, phase transitions.

1.- INTRODUCTION

Knowledge of the crystalline structures and phase transitions of mixed rare earth disilicates (RE, RE') Si_2O_7 is essential to understand their properties in the fields of advanced ceramics sintering and optical materials. Rare-earth disilicates $RE_2Si_2O_7$ (RE = lanthanides, Sc and Y) are well known for their polymorphism (Felsche, 1973). They exhibit seven structure types at normal pressure, known as A, B, C, D, E, F, and G, depending on the temperature and the ionic radius of the RE cation. $Y_2Si_2O_7$ shows, in addition to the B (or α), C (or β), D (or γ) and E (or δ), a low temperature form known as *y*-polymorph or yttrialite (Ito and Johnson, 1968).

Rare-earth disilicates have been studied during the past decades because of applied and basic interests. First they were studied because of their unique magnetic, electrical and optical properties, making them interesting materials for e.g. the application in microwave technology, ferromagnetics, lasers and phosphors (Felsche, 1973; Liddel and Thompson, 1986). More recently, the interest in these materials has been renewed because they appear as secondary phases after sintering Si_3N_4 and SiC ceramics using rare-earth oxides as sintering additives. The properties of the sintered materials are strongly influenced by the type and content of their secondary phases (Cinibulk and Thomas, 1992; Kumar and Drummond, 1992; Choi et al. 1999; Klemm, 2002; Matovic et al. 2004; Lojanova et al. 2010). Several rare-earth disilicates are currently studied for the possible use as environmental barrier coatings for the protection of structural ceramics in severely corrosive environments (Aparicio and Duran, 2000; Lee et al., 2005; Suetsuna and Ohji, 2005; Maier et al. 2007). Finally, Pomeroy et al. (2005) have demonstrated that the stability and glass properties of different SiAlON glasses doped with rare earths depend on the relative stability of the different rare earth disilicate phases that form after treatment at high temperature. Many of these applications use mixtures of RE to improve the properties of the final material (Hirosaki et al., 1988; Hirosaki and Okada, 1992; Pomeroy et al. 2005; Marchi et al. 2009). For example, Chen et al. (1997) found that when the ratio Y_2O_3/La_2O_3 changed from 1/3 to 3/1, the predominant crystalline phase of the corresponding oxyinitride glass was changed from a solid solution of $(La,Y)_5(SiO_4)_3N$ (H-phase) to a partial solid solution of $(La,Y)_2Si_2O_7$ after annealing the glasses at 1500ºC. $(La,Y)_2Si_2O_7$ (RE=La,Y) has a smaller thermal expansion coefficient and higher oxidation resistance than the H-phase, so its

occurrence at the grain boundaries would be of benefit for the high temperature mechanical and chemical properties of Si_3N_4 ceramics. Knowledge of the crystalline structures adopted by the $(RE,RE`)_2Si_2O_7$ phases at different temperatures and RE contents is therefore of great value in understanding the behaviour and properties of these materials.

Solid solubility between disilicates of different rare earths has been reported in the literature (Ito and Johnson, 1968; Monteverde and Celotti, 1999 and 2002; Becerro and Escudero 2005a, 2005b, 2006; Maier et al. 2006; Escudero at al. 2007; Ohashi et al. 2007). There is clear evidence that the incorporation of rare earths of one type into the disilicate of a RE of another type has a strong influence on the stability of the different polymorphs. Pomeroy et al. (2005) and Maier et al. (2006) suggested and demonstrated, respectively, that the phase stabilities of a disilicate solid solution behave just like the phase stabilities of a silicate with RE ionic radius equal to the average of the radii of the rare earths in the solid solution ("radius criterion"). However, most of the studies they based their analysis on were carried out in $RE_2Si_2O_7$-$RE`_2Si_2O_7$ systems that show, at least, one common polymorph.

The only structural study found in the literature of $RE_2Si_2O_7$-$RE´_2Si_2O_7$ systems that do not show any common polymorph is that from Monteverde and Celotti (1999). These authors studied the solid solubility of $La_2Si_2O_7$ and $Y_2Si_2O_7$ at 1600ºC, and described the structure of $(Y_{2/3}La_{1/3})_2Si_2O_7$ as isostructural with G-$La_2Si_2O_7$. However, the synthesis had to be made with an excess of amorphous silica in the initial mixture in order to obtain the desired phase. As a result, the XRD pattern of the product contained an α-cristobalite reflection four times more intense than the most intense reflection of the pursued La-Y disilicate phase, with the consequent uncertainty in the phase stability of the silicate as well as in the subsequent structure refinement.

The present study provides new information for a better understanding of the phase stabilities in the $La_2Si_2O_7$ and $Y_2Si_2O_7$ system. We have selected the 50% composition of the system ($La_{1.0}Y_{1.0}Si_2O_7$) and examined structures and phase transitions as a function of temperature, as well as conversion kinetics. The synthesis method used here allowed obtaining the disilicate phase as the major product (> 90 wt %). The behaviour of the compound versus temperature will be compared with those of the rare earth

disilicates with RE ionic radius similar to the average of the radii of the rare earths in the solid solution, in order to check the proposed "radius criterion". Finally, mechanical properties of the high temperature polymorph (G-$La_{1.0}Y_{1.0}Si_2O_7$) will be presented and compared with related ceramics.

2.- EXPERIMENTAL

2.1.- Sol-gel synthesis: The $La_{1.0}Y_{1.0}Si_2O_7$ composition was synthesised following a sol-gel route. Starting reagents were $La(NO_3)_3.6H_2O$ (99,99% Aldrich Chemical Co.), $Y(NO_3)_3.6H_2O$ (99,99% Aldrich Chemical Co.) and $Si(OC_2H_5)_4$ (TEOS, 99% Aldrich Chemical Co.). A TEOS solution in ethanol (1:3 in volume) was added over the appropriate amounts of $La(NO_3)_3.6H_2O$ and $Y(NO_3)_3.6H_2O$ and dissolved in 5 ml of absolute ethanol. Addition of a slight excess (10% volume) of TEOS in the initial mixture was necessary to obtain satisfactorily the $La_{1.0}Y_{1.0}Si_2O_7$ phase. The mixture was stirred at 40 ºC for ~ 7 hours and the white gel obtained was dried at 60 ºC for 24 h in air. Nitrates were eliminated by calcination at 500ºC for 2 h at heating rate of 1 ºC·min^{-1}.

2.2.- Calcination experiments: The xerogel obtained was ground in an agate mortar and subsequently divided into different portions. They were submitted to heat treatment in air at temperatures between 1100º C and 1650 ºC and calcination times from 12 hours to 21 days, with a heating rate of 5 ºC·min^{-1}, using a platinum crucible. Finally, the samples were slowly cooled down to room temperature.

2.3.- Characterization: The global composition of the sample was examined by EDX spectroscopy with a NORAN germanium detector installed in an ATEM, Philips CM20 FEG, obtaining a Y/La molar ratio of 0.99(0.05), which agrees with the $La_{1.0}Y_{1.0}Si_2O_7$ nominal stoichiometry. These analyses were registered in selected single crystals of the sample. The powdered sample was dispersed in ethanol by sonication and dropped on a conventional carbon-coated copper grid. TEM and selected area electron diffraction was also used to study the symmetry of the different polymorphs. The EDA program (Kogure, 2003) was used to index the electron diffraction patterns.

X-Ray diffraction (XRD) patterns were recorded in two types of diffractometers:

1) PANalytical X`Pert Pro Diffractometer (CuK_α) with an X-Celerator detector over an angular range of $10^o < 2\theta < 120^o$, 2θ step width of 0.02^o and 10 s counting time.

2) High-intensity and high-resolution *synchrotron powder XRD* data have been recorded on the 11-BM diffractometer at the Advanced Photon Source (APS), Argonne National Laboratory. Data were collected over the 0.5-55° 2θ range with a 0.001°step size at room temperature using a wavelength of λ=0.413581Å. The sample was contained in a 0.5 mm capillary and was spun at 60 Hz during data collection.

In both cases, the patterns were analyzed using both Le Bail and Rietveld methods with the JANA software (Petricek et al. 2006). Refined parameters were: background coefficients, zero error, scale factors, unit cell parameters, microstructural parameters, site occupation factors for the rare earth sites, isotropic atomic displacement parameters, and atomic positions.

^{29}Si Magic Angle Spinning Nuclear Magnetic Resonance (MAS NMR) spectroscopy was carried out in a Bruker DRX400 Avance (9.39 T) spectrometer equipped with a multinuclear probe, using 4 mm zirconia rotors spinning at 10 kHz. A single pulse sequence was used, with an observation frequenzy for ^{29}Si of 79.49 MHz, a pulse width of 2.5 μs ($\pi/2$ pulse length = 7.5 μs) and a delay of 300s. Chemical shifts are reported in ppm from tetramethylsilane (TMS). The experimental ^{29}Si NMR spectra were fitted using a modified version of the Bruker Winfit program, which handles the finite spinning speed in MAS experiments (Massiot et al., 2002).

A high density pellet of G-$La_{1.0}Y_{1.0}Si_2O_7$ was obtained with the following method: the corresponding xerogels was ball milled with 4 wt% $LiYO_2$ (sintering aid) in isopropyl alcohol for 6 hours using Si_3N_4 milling media. After drying, the powder was first compacted in a uniaxial press (5 ton, 5 min.) and the resulting pellet was finally compacted in a cold isostatic press at 200 MPa for 5 min. The pellet was calcined at 1650 ºC for 2 hours using a Pt crucible and a heating/cooling rate of 5 ºC $\cdot min^{-1}$. In case of sintering with additive, 4 wt% $LiYO_2$ was used. The microhardness was determined using the indentation technique (Buehler, model Micromet 5103, Düsseldorf, Germany) with a conventional diamond pyramid indenter and the diagonals of each indentation were measured using an optical microscope. The pellet was previously polished with

diamond to 1 μm (Struers, model RotoPol-31, Alcobendas- Madrid, Spain). Measuring conditions for the Vickers hardness, Hv, were an applying load of 100 N for 10 s and the standard specification ASTM E92-72 (Antis et al., 1981). The value of Hv is the relationship between the applied load P and the surface area of the diagonals of indentation. Fifty indentations were made on the sample, and the results were averaged. The fracture toughness (K_{IC}) was estimated from the length of the cracks of the residual print. The Anstis et. al (1981) equation for pyramidal indenter geometry was used to calculate the K_{IC} value:

$$K_{ic} = 0.016\left(\frac{E}{H}\right)^{0.5}\frac{P}{C^{3/2}}$$

where *E* is the Young`s module, *H* is the hardness, *P* (in mN) is the peak indentation load, and *C* (in mm) is the length of the radial cracks. To calculate K_{ic} the value of (E/H) in expression 1 was set to 25, which is approximately true for ceramic materials (Dusza and Sajgalik, 1995).

3.- RESULTS

3.1.- Polymorphism with temperature

The average ionic radius of the rare earths in $La_{1.0}Y_{1.0}Si_2O_7$ is 1.090 Å, which is very close to the Pm^{3+} ionic radius (1.093 Å). There are no crystallographic data on $Pm_2Si_2O_7$ due to the fact that Pm is a radioactive element. The Sm^{3+} and Nd^{3+} cations show ionic radii just below and above Pm^{3+} (respectively 1.079 Å and 1.109 Å).[†] Following the phase diagram published by Felsche (1973), $Sm_2Si_2O_7$ suffers the following phase transitions with temperature:

$$\underset{\text{Tetragonal } (P4_1)}{\text{A-}Sm_2Si_2O_7} \xrightarrow{1525\ ^oC} \underset{\text{Monoclinic } (P2_1/c)}{\text{G-}Sm_2Si_2O_7} \xrightarrow{1575\ ^oC} \underset{\text{Triclinic } (P\bar{1})}{\text{F-}Sm_2Si_2O_7}$$

On the other hand, $Nd_2Si_2O_7$ displays dimorphism, with the following polymorphs and transition temperature:

[†] The ionic radius values given correspond to the 3+ cations with coordination number VIII, as expected in most of the RE crystallographic sites of the $Sm_2Si_2O_7$ and $Nd_2Si_2O_7$ polymorphs (Felsche, 1973). Ionic radii have been taken from Shannon (1976).

$$\underset{\text{Tetragonal } (P4_1)}{\text{A-Nd}_2\text{Si}_2\text{O}_7} \xrightarrow{1475\ ^{o}\text{C}} \underset{\text{Monoclinic } (P2_1/c)}{\text{G-Nd}_2\text{Si}_2\text{O}_7}$$

G-$Nd_2Si_2O_7$ is the stable phase up to the melting point of the compound. In order to follow the "radius criterion" explained above, $La_{1.0}Y_{1.0}Si_2O_7$ would be expected to transform from tetragonal (A-polymorph) to monoclinic (G-polymorph) symmetry at a temperature in between 1475 ºC and 1525 ºC. At higher temperatures it could also transform into the triclinic F-polymorph, as reported for $Sm_2Si_2O_7$.

Table 1 shows the polymorphs observed after calcination of the $La_{1.0}Y_{1.0}Si_2O_7$ composition at temperatures between 1100 ºC and 1600 ºC for several days, derived from the analysis of the conventional XRD patterns. The XRD pattern of the sample calcined at 1100 ºC for 4 days is compatible with PDF card 04-009-9536 (A-$La_2Si_2O_7$, tetragonal $P4_1$) with some differences in the intensity and position of the reflections. These differences are due to the different atomic form factor curves of La^{3+} and Y^{3+} as well as to the different unit cell sizes. This behaviour is in agreement with the radius criterion, since both $Sm_2Si_2O_7$ and $Nd_2Si_2O_7$ show also tetragonal symmetry at 1100 ºC. When the sample is calcined two more days at 1100 ºC, the XRD pattern is still dominated by reflections of the A-$RE_2Si_2O_7$ polymorph. However, some low intensity reflections appear, which match PDF card 01-082-0729 (G-$La_2Si_2O_7$, monoclinic $P2_1/c$), also with slight differences in position and intensity. Increasing calcination time at 1100 ºC favours transformation of A- into G-$RE_2Si_2O_7$, but 21 days are not sufficient for a complete transformation, as will be described below. Again, the fact that the reflections are slightly shifted from those of G-$La_2Si_2O_7$, with different intensity ratios, indicates that a solid solution of $Y_2Si_2O_7$ in G-$La_2Si_2O_7$ is formed in these conditions. Calcination at 1200 ºC produces also A-$RE_2Si_2O_7$ (RE=La, Y) after short calcination times, with transformation to G-$RE_2Si_2O_7$ (RE= La, Y) after longer calcination periods. In this case, complete A to G transformation is attained after 11 days. The kinetics of the A to G polymorph transformation will be studied below. Finally, only G-$RE_2Si_2O_7$ is obtained when calcination is carried out at temperatures of 1250 ºC and higher, whatever the duration of the calcination is. These results demonstrate that G-$RE_2Si_2O_7$ (RE=La, Y) is the stable polymorph in the whole temperature range and that, therefore, the $La_2Si_2O_7$-$Y_2Si_2O_7$ system does not obey the radius criterion.

3.2.- Study of the tetragonal A-$La_{1.0}Y_{1.0}Si_2O_7$ phase

The XRD pattern of the sample annealed at 1200 ºC for 1 day (crosses in Figure 1) matches PDF card 04-009-9536 corresponding to A-$La_2Si_2O_7$. All reflections appear slightly shifted with respect to the mentioned card, due to changes in unit cell dimensions as contents. The reflections are broad in general and not well resolved, indicating a low degree of crystallinity. Attempts to improve crystallization by increasing calcination time resulted in the transformation of the tetragonal to the monoclinic polymorph of $RE_2Si_2O_7$, as described above. In fact, very few reflections of low intensity, corresponding to G-$RE_2Si_2O_7$ (RE=La, Y) (PDF card 01-082-0729, G-$La_2Si_2O_7$), are also observed in the XRD pattern. Low intensity reflections of a third phase are also observed corresponding to the apatite-type phase $Y_{4.67}(SiO_4)_3O$ (PDF 04-006-9901). Unit cell parameters were calculated using the LeBail method. Rietveld refinement was not carried out in this case due to the low to avoid an erroneous structure solution. The fitting included A-$(La,Y)_2Si_2O_7$, G-$(La,Y)_2Si_2O_7$ and apatite phases. Starting unit cell parameters were taken from those reported for A-$La_2Si_2O_7$ (Müller-Bunz and Schleid, 2000) with space group $P4_1$, G-$La_2Si_2O_7$ (Christensen, 1994) with space group $P2_1/c$, and apatite (Maksimov et al. 1969) with space group $P6_3/m$. Figure 1 (solid line) shows the fitted pattern and the difference curve. Unit cell parameters obtained for A-$(La,Y)_2Si_2O_7$ were a= 6.7664(2) Å and c= 24.6868(8) Å, to be compared to 6.8383(7) and 24.7360(40) obtained by Müller-Bunz and Schleid (2000) for the A-$La_2Si_2O_7$ end-member. This result indicates that Y^{3+} enters the La^{3+} crystallographic site, producing a decrease in the unit cell parameters as a consequence of the lower ionic radius of Y^{3+} compared to La^{3+}.‡ TEM/EDX spectra carried out in different tetragonal single crystals confirm the presence of both cations in the crystal (Figures 2a, 2b and 2c).

3.3.- Study of the monoclinic G-$La_{1.0}Y_{1.0}Si_2O_7$ phase.

Synchrotron XRD has been recorded on the sample annealed at 1600 ºC for 2 days to analyze the structure of the monoclinic G-$La_{1.0}Y_{1.0}Si_2O_7$ phase using the Rietveld method. Starting parameters were those described for G-$La_2Si_2O_7$ (Christensen, 1994)

‡ The extremely irregular coordination polyhedra around each of the four crystallographically independent RE^{3+} cations in A-RE2Si2O7 consist of 9 and 8 oxygen atoms (two polyhedra of each type). Ionic radii (Å) in VIII and IX coordination, respectively, are the following: Y^{3+} (1.019, 1.075) and La^{3+} (1.160, 1.216) (Shannon, 1976).

using space group $P2_1/c$. The La/Y ratio has been refined on each of the two rare-earth crystallographic sites present in the monoclinic cell. The global composition has been constrained to its nominal value (La/Y=1.0). Cristobalite has been added as secondary phase (less than 8 wt.%). Figure 3 shows the experimental, fitted and difference curves. All the reflections could be fitted on the basis of a monoclinic cell with space group $P2_1/c$. Unit cell parameters obtained were a= 5.3817(1)Å, b= 8.6029(1)Å, c= 14.0324(2)Å, and β=113.212(1)°. Atomic parameters and interatomic distances can be found in Table 2a and 2b, respectively.

Figure 4 shows the unit cell volume of several G-$RE_2Si_2O_7$ compounds (RE= Sm, Nd, Pr, Ce and La) as a function of the RE ionic radius, taken from Felsche (1973). The unit cell volume of the G- $La_{1.0}Y_{1.0}Si_2O_7$ phase calculated in the Rietveld fit (597.060(3) $Å^3$) has also been plotted versus the ionic radius expected from the average of the ionic radii in $La_{1.0}Y_{1.0}Si_2O_7$. This data point perfectly fits in the regression line described by the other G-$RE_2Si_2O_7$ compounds. This fact demonstrates that a solid solution of $Y_2Si_2O_7$ in G-$La_2Si_2O_7$ is formed at the 50% composition, with formation of G-$La_{1.0}Y_{1.0}Si_2O_7$. Site occupation factors of La and Y (Table 2) indicate that La occupies preferentially the rare earth crystallographic site 1 while Y is located in the rare earth site 2. Pure G-$RE_2Si_2O_7$ compounds (RE=Sm, Nd, Pr, Ce and La) show larger RE-O distances for RE site 1 compared to RE site 2. The bigger ionic radius of La^{3+} compared to Y^{3+} could explain the observed inhomogeneous distribution of both cations. In fact, the average La1/Y1-O distance is bigger than the La2/Y2-O one (see Table 2b).

Figure 5a shows the ^{29}Si MAS NMR spectrum of the sample annealed at 1600 ºC for 2 days. It consists of a unique band with a slight asymmetry towards high frequencies. The band must be composed of two Si resonances corresponding to the two different Si crystallographic sites in the monoclinic G-$La_{1.0}Y_{1.0}Si_2O_7$ unit cell. The spectrum has been simulated with two resonances plus an additional one to fit the asymmetry observed at high frequencies. The results of the fitting have been included in Table 3. The area under the curve of the resonances corresponding to Si in G-$La_{1.0}Y_{1.0}Si_2O_7$ are very similar to each other, as expected from the same occupation of both crystallographic sites in the monoclinic unit cell. However, the fwhm is bigger in one of the sites, indicating a higher degree of disorder around that Si site. In fact, the Si-O distances obtained from the structure refinement described above show a higher

dispersion of values at the Si1 tetrahedron compared to Si2 tetrahedron (see Table 2b). Finally, the low intensity band at high frequency (-82.4 ppm) can be assigned to small nuclei of δ-$La_{1.0}Y_{1.0}Si_2O_7$ of insufficient domain size as to be observed by diffraction.

Dupree et al. (1989) reported the ^{29}Si NMR spectrum of a mixture of apatite ($La_{4.67}Si_3O_{13}$) and G-$La_2Si_2O_7$ (called h-$La_2Si_2O_7$ in that paper). The spectrum consisted of two signals at -77.7 ppm and -82.6 ppm (280 Hz fwhm) that the authors assigned, respectively, to apatite and G-$La_2Si_2O_7$. The fact that a unique signal is observed for h-$La_2Si_2O_7$, in spite of the two different Si crystallographic sites in G-$La_2Si_2O_7$ must be due to the low resolution of the spectrum. We have synthesized apatite-free G-$La_2Si_2O_7$ following the same procedure described above for G-$La_{1.0}Y_{1.0}Si_2O_7$. The ^{29}Si MAS-NMR spectrum is shown in Figure 5b. It shows a band with two maxima at -83.8 ppm and -82.7 ppm and fwhm values of 95 Hz each, corresponding to the two Si sites in the monoclinic unit cell of G-$La_2Si_2O_7$. The third contribution (9 % of the total area) at -81.7 ppm corresponds to Si in a structure that is not detected by XRD. Comparing the ^{29}Si chemical shift values of G-$La_2Si_2O_7$ with those of G-$La_{1.0}Y_{1.0}Si_2O_7$ (Table 3) it can be observed that introducing Y in the La site shifted the signals towards lower frequency values. This fact has been assigned to differences in electronegativity of the rare earth cations in the second coordination shell of Si (Janes and Oldfield, 1985; Becerro and Escudero 2005b; Ohashi et al. 2007). Finally, introducing Y in the La sites creates a high degree of local disorder around the Si atoms, as inferred from the differences in fwhm values between G-$La_2Si_2O_7$ and G-$La_{1.0}Y_{1.0}Si_2O_7$ (Table 3). This behaviour has also been observed in related systems such as $Lu_2Si_2O_7$-$Y_2Si_2O_7$ (Becerro and Escudero, 2005a) and $Sc_2Si_2O_7$-$Y_2Si_2O_7$ (Escudero et al. 2007).

3.4.- A- to G-$La_{1.0}Y_{1.0}Si_2O_7$ transition kinetics

The A-$RE_2Si_2O_7$ to G-$RE_2Si_2O_7$ phase transition is a reconstructive type transition according to the differential thermal analysis data of Felsche (1973) for pure $RE_2Si_2O_7$ compounds. Reconstructive transitions involve a reorganization of the crystal structure that is achieved by breaking and reforming coordination bonds. These transitions typically have large activation energies and are kinetically very sluggish. Felsche (1973) observed large variations in time, from 30 min. to ∞, for the individual transitions in pure $RE_2Si_2O_7$ compounds. "∞" means not converted within a reasonable period of

time, i.e. within 100 hours of observation. The low diffusion rate of the ions involved in the "reconstructive transitions" sometimes resulted in the coexistence of two corresponding modifications. A kinetic study of such transitions has not been published up to now.

Figure 6a represents the fraction of G-$La_{1.0}Y_{1.0}Si_2O_7$ versus calcination time at 1100 ºC and 1200 ºC. Quantification has been obtained from the XRD patterns of the samples using the Rietveld method. The sluggishness of the reaction can be inferred from these data, which indicate that the phase transition needs ca. 250 hours to be completed at 1200ºC, while complete transformation was not observed after 21 days calcination at 1100 ºC. This explains the observations of Felsche (1973) commented above. The plot at 1200ºC clearly shows a sigmoidal form, the reaction rate being small at the beginning, then increasing to a maximum, and finally decreasing to zero as the reaction goes to completion. It is well known that the isothermal kinetics of a wide range of mineral reactions, which include reconstructive polymorphic transformations, can be described by an Avrami equation of the type:

$$y = 1 - \exp(-kt)^n \qquad (1)$$

where *y* is the fraction transformed, *k* is a rate constant and *n* is a constant that depends on the reaction mechanism. To extract values of the rate constant *k* from equation 1, the usual approach is to linearize the equation to get

$$\ln(-\ln(1-y) = n\ln k + n\ln t \qquad (2)$$

Thus, a reaction whose kinetics conform to this Avrami equation gives a straight line when ln(-ln(1-*y*)) is plotted against ln *t*. Figure 6b shows the data for the A- to G-$La_{1.0}Y_{1.0}Si_2O_7$ transformation against ln *t* at 1200 ºC. Values for *n* and *k* were *n*= 4 and *k* = $4.4 \cdot 10^{-3}$ h^{-1}. The physical interpretation of the Avrami constants, *k* and *n*, is difficult and it is still open to interpretation. According to the original theory, *n* should be an integer from 1 to 4, the value of which should depend only on the type of the statistical model; however, it has become customary to regard it as an adjustable parameter that may be non-integral. The value of 4 can be interpreted as nuclei non-preformed and growing at a constant nucleation rate in the three dimensions (Jena and Chaturvedi, 1992).

On the other hand, transformation at lower temperatures was much slower, as seen in Figure 6a for the 1100 ºC case. Therefore, the rate constant could not be calculated for that isotherm. Finally, calcination at 1250 ºC and above yielded the G-$La_{1.0}Y_{1.0}Si_2O_7$ polymorph directly.

3.5.- Does G-$La_{1.0}Y_{1.0}Si_2O_7$ transform to F-$La_{1.0}Y_{1.0}Si_2O_7$ at high temperature?

Sm^{3+} and Nd^{3+} show ionic radii (1.079 Å and 1.109 Å, respectively) just below and above the average radius the rare earths in $La_{1.0}Y_{1.0}Si_2O_7$ (1.090 Å). It has been reported that G-$Sm_2Si_2O_7$ transforms into F- $Sm_2Si_2O_7$ (P-1 space group) at 1575ºC, while G-$Nd_2Si_2O_7$ is the stable polymorph up to the melting point of the compound (Felsche, 1973). G- and F-$RE_2Si_2O_7$ are extremely similar and difficult to distinguish by powder X-ray diffraction.

In order to check whether G-$La_{1.0}Y_{1.0}Si_2O_7$ transforms into F-polymorph or not, a sample of G-$La_{1.0}Y_{1.0}Si_2O_7$ was calcined at 1650 ºC for 12 hours. The XRD pattern was very similar to that of the sample annealed at 1600 ºC (Figure 7). However, convergence could be achieved when refining using both models, hindering the determination of this possible phase transition. Both structures can however be distinguished by selected area electron diffraction patterns taken on the TEM. Figure 8a shows a silicate grain of the sample calcined at 1650ºC with its corresponding electron diffraction pattern (Figure 8b). Most of the electron diffraction patterns of the different silicate grains could be indexed according to both the monoclinic and triclinic symmetry. However, the electron diffraction pattern taken along the [010] zone axis considering the monoclinic structure can be distinguished from its analogous pattern taken along the [100] zone axis if the triclinic structure is considered. Both simulations are shown in Figure 8c and 8d, respectively. It can be observed that the (001) and (100) families of planes appear on the electron diffraction pattern of the triclinic structure (Figure 9b) but the analogous spots do not appear on the pattern when the monoclinic symmetry is considered. The experimental pattern presented in Figure 8b is compatible with the one corresponding to the monoclinic symmetry. This demonstrates that $La_{1.0}Y_{1.0}Si_2O_7$ keeps the monoclinic structure of the G polymorph and does not transform into the F polymorph, at least at $T \leq 1650$ºC. The fact that $Sm_2Si_2O_7$ displays three different polymorphs with temperature reflects the rather unstable $4f^5$ electronic

configuration of the Sm^{3+} cation. On the contrary, the stability of the La^{3+} ($4f^0$) and Y^{3+} ($3d^{10}$) electronic configurations favours the existence of only one stable polymorph in $La_{1.0}Y_{1.0}Si_2O_7$, in spite of the similar value of the average ionic radius of the rare earths in this compound compared to the ionic radius of Sm^{3+}.

3.6.- Mechanical properties of the high temperature polymorph G-$La_{1.0}Y_{1.0}Si_2O_7$.

The measured mechanical properties of G-$La_{1.0}Y_{1.0}Si_2O_7$ are summarized in Table 4, together with those of pure γ-$Y_2Si_2O_7$ (Sun et al. 2007), the initial materials SiO_2 and Y_2O_3 and Macor, a typical machinable ceramic. The introduction of La in the $Y_2Si_2O_7$ structure increases the hardness value from 6.2 ± 0.1 to 7.0 ± 0.3, although the fracture toughness decreases slightly. Although the values for the mechanical properties of La_2O_3 could not be found in the literature, it can be observed that the values for G-$La_{1.0}Y_{1.0}Si_2O_7$ are slightly higher than the average of the silicon and yttrium oxides. Finally, the high fracture toughness suggests that G-$La_{1.0}Y_{1.0}Si_2O_7$ could be a good damage-tolerant ceramic, similar to Macor, as demonstrated by Sun et al. (2007) for γ-$Y_2Si_2O_7$.

Conclusions

Y enters the La sites in both A-$(La,Y)_2Si_2O_7$ and G-$(La,Y)_2Si_2O_7$ structures forming solid solutions. A-$(La,Y)_2Si_2O_7$ is not a thermodynamically stable phase and the "radius criterion" is not obeyed in this rare earth disilicate system. La occupies preferentially the rare earth crystallographic site 1 while Y is located in the rare earth site 2 in the G-$(La,Y)_2Si_2O_7$ structure. The incorporation of Y creates a high degree of local disorder around the Si atoms. The A- to G-$La_{1.0}Y_{1.0}Si_2O_7$ phase transition is extremely sluggish. It needs ca. 250 hours to be completed at 1200ºC, while complete transformation was not observed after 21 days calcination at 1100 ºC. Transformation of G- to F-$(La,Y)_2Si_2O_7$ at high temperature was not observed in this composition. The high fracture toughness suggests that G-$La_{1.0}Y_{1.0}Si_2O_7$ could be a good damage-tolerant ceramic.

Acknowledgements

A.J. Fernandez-Carrion gratefully acknowledges an F.P.D.I. grant from Junta de Andalucía. Supported by DGICYT (Project no. CTQ2010-14874/BQU) and Junta de Andalucía (FQM-6090).

References

Antis G.; Chantikul P.; Lawn B.; Marshall D. *J. Am. Ceram. Soc.* **1981**, *64*, 533.

Aparicio M.; Duran A. *J. Am. Ceram. Soc.* **2000**, *83*, 1351.

Becerro A.I.; Escudero A. *Chem. Mater.* **2005a**, *17*, 112.

Becerro A.I.; Escudero A. *J. Solid State Chem.* **2005b**, *178*, 1.

Becerro A.I.; Escudero A. *J. Eur. Ceram. Soc.* **2006**, *26*, 2293.

Chen J.; Wei P.; Huang Y. *J. Mater. Sci. Lett.* **1997**, *16*, 1486.

Choi H.J.; Lee J.G.; Kim Y.W. *J. Eur. Ceram. Soc.* **1999**, *19*, 2757.

Christensen N.A. *Z. Kristallogr.* **1994,** *209*, 7.

Cinibulk M.K.; Thomas G. *J. Am. Ceram. Soc.* **1992**, *75*, 2044.

Dupree R.; Lewis M.H.; Smith M.E. *J. Am. Chem. Soc.* **1989**, *111*, 5125.

Dusza J.; Sajgalík P. Handbook of Advanced Materials Testing in Fracture Toughness and Strength Testing of Ceramic Composites, cap. 25. Marcel Dekker, inc, 554-560, **1995**.

Escudero A.; Alba M.D.; Becerro A.I. *J. Solid State Chem.* **2007**, *180*, 1436.

Felsche J. *Struct. Bond.* **1973**, *13*, 99.

Hirosaki N.; Okada A.; Matoba K. *J. Am. Ceram. Soc.* **1988**, *71*, C-144.

Hirosaki N.; Okada A. *J. Mat Sci.* **1992**, *27*, 3743.

Ito J.; Johnson H. *Am. Mineral.* **1968**, *53*, 1940.

Janes N.; Oldfield E. *J. Am. Chem. Soc.* **1985**, *107*, 6769.

Jena A.K.; Chaturvedi M.C. Phase Transformations in Materials. Prentice Hall. 1992, pp 243-247.

Klemm H. *J. Eur. Ceram. Soc.* **2002,** *22*, 2735.

Kogure, T. *J. Cryst. Soc. Japan* **2003,** *45*, 391.

Kumar S.; Drummond C.H. *J. Mater. Res.* **1992**, *7*, 997.

Lee K.N.; Fox D.S.; Bansal N.P. *J. Eur. Ceram. Soc.* **2005**, *25*, 1705.

Liddell K.; Thompson D.P., *Br. Ceram. Trans.* **1986**, *85*, 17.

Lojanova S.; Tatarko P.; Chlup Z.; Hnatko M.; Dusza J.; Lences Z.; Sajgalik P. *J. Eur. Ceram. Soc.* **2010**, *30*, 1931.

Maier N.; Rixecker G.; Nickel K.G. *J. Solid State Chem.* **2006**, *179*, 1630.

Maier N.; Nickel K.G.; Rixecker G. *J. Eur. Ceram. Soc.* **2007**, *27*, 2705.

Marchi J.; Chaves Guedes e Silva C.; Batista Silva B.; Bressiani J.C.; de Almeida Bressiani A.H. *Mater. Res*. **2009**, *12*, 145

Massiot D.; Fayon F.; Capron M.; King I.; Le Calvé S.; Alonso B.; Durand J.O.; Bujoli B.; Gan Z.; Hoatson G. *Magn. Reson. Chem.* **2002**, *40*, 70.

Matovic B.; Rixecker G.; Aldinger F. *J. Eur. Ceram. Soc.* **2004,** *24*, 3395.

Maksimov B.A.; Litvin B.N.; Iliukhin V.V.; Belov N.V. *Sov. Phys. Crystallogr. (Engl. Transl.)* **1969**, *14*, 407.

Monteverde F.; Celotti G. *J. Eur. Ceram. Soc.* **1999**, *19*, 2021.

Monteverde F.; Celotti G. *J. Eur. Ceram. Soc.* **2002**, *22*, 721.

Müller-Bunz H.; Schleid T. *Z. Anorg. Allg. Chem.* **2000**, *626*, 2549.

Ohashi H.; Alba M.D.; Escudero A.; Becerro A.I. *J. Phys. Chem. Solids* **2007**, *68*, 464.

Petricek V.; Dusek M.; Palatinus L. Institute of Physics, Academy of Sciences of the Czech Republic, Praha. **2006**. http://www-xray.fzu.cz/jana/jana.html.

Pomeroy M.J.; Nestor E.; Ramesh R.; Hampshire S. *J. Am. Ceram. Soc.* **2005**, *88*, 875.

Shannon R.D. *Acta Crystal. A* **1976**, *32*, 751.

Suetsuna T.; Ohji T. *J. Am. Ceram. Soc.* **2005**, *88*, 1139.

Sun Z.; Zhou Y.; Wang J.; Li M. *J. Am. Ceram. Soc.* **2007,** *90*, 2535.

Figures

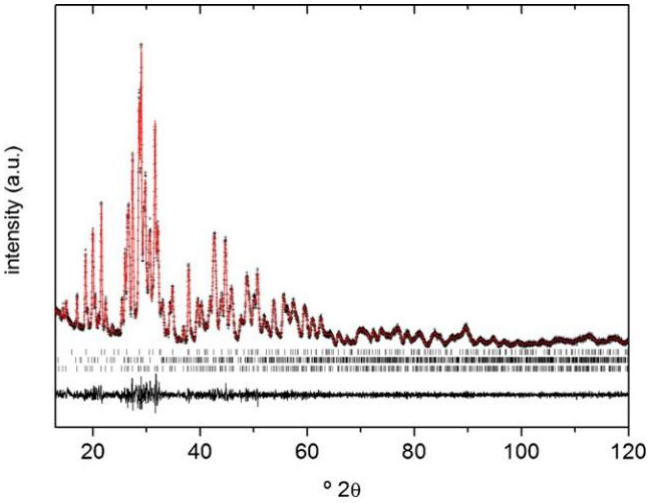

Figure 1: Experimental (crosses) and calculated (solid line) XRD (CuK_α radiation) pattern of $La_{1.0}Y_{1.0}Si_2O_7$ annealed at 1200 ºC 1 day. The difference plot is also shown. Bottom tick marks: A-$RE_2Si_2O_7$; Middle tick marks: G-$RE_2Si_2O_7$; Top tick marks: apatite-like silicate.

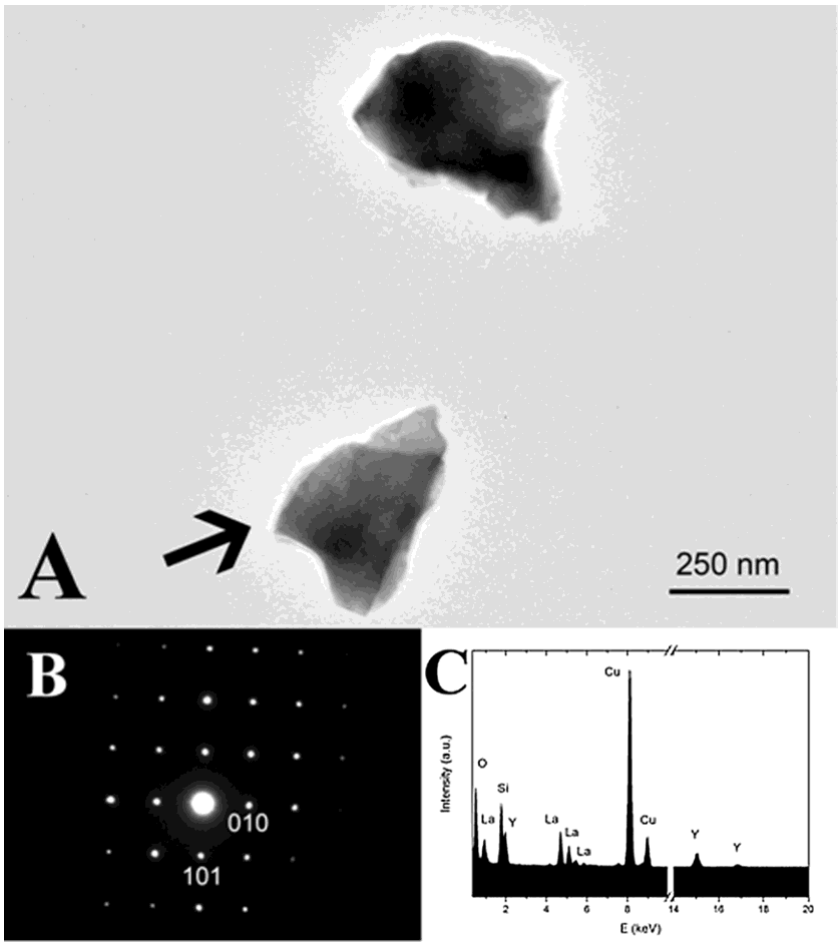

Figure 2: A) Bright field TEM micrograph of two $La_{1.0}Y_{1.0}Si_2O_7$ grains of the sample calcined at 1200ºC for 24 hours. B) Electron diffraction pattern of the grain marked with an arrow in A. The pattern has been indexed along the [-101] zone axis of the tetragonal A-$La_{1.0}Y_{1.0}Si_2O_7$. C) EDX corresponding to the same single crystal.

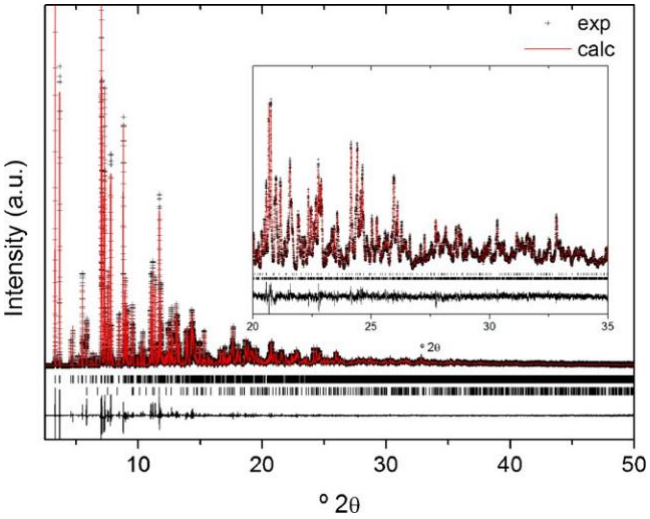

Figure 3: Experimental (crosses) and calculated (solid line) XRD pattern (11BM synchrotron radiation) of $La_{1.0}Y_{1.0}Si_2O_7$ annealed at 1600 ºC for 2 days. The difference plot is also shown. Bottom tick marks: G-$RE_2Si_2O_7$, top tick marks: cristobalite.

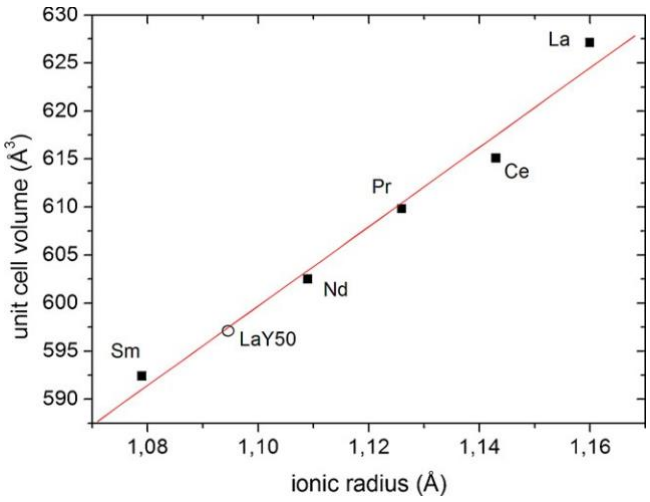

Figure 4: Solid circles: Unit cell volume of different G-$RE_2Si_2O_7$ compounds (RE=Sm, Nd, Pr, Ce and La) versus the ionic radius of the RE^{3+} with VIII coordination. Open circle: Unit cell volume of G-$La_{1.0}Y_{1.0}Si_2O_7$ calculated by Rietveld fit of the corresponding XRD pattern.

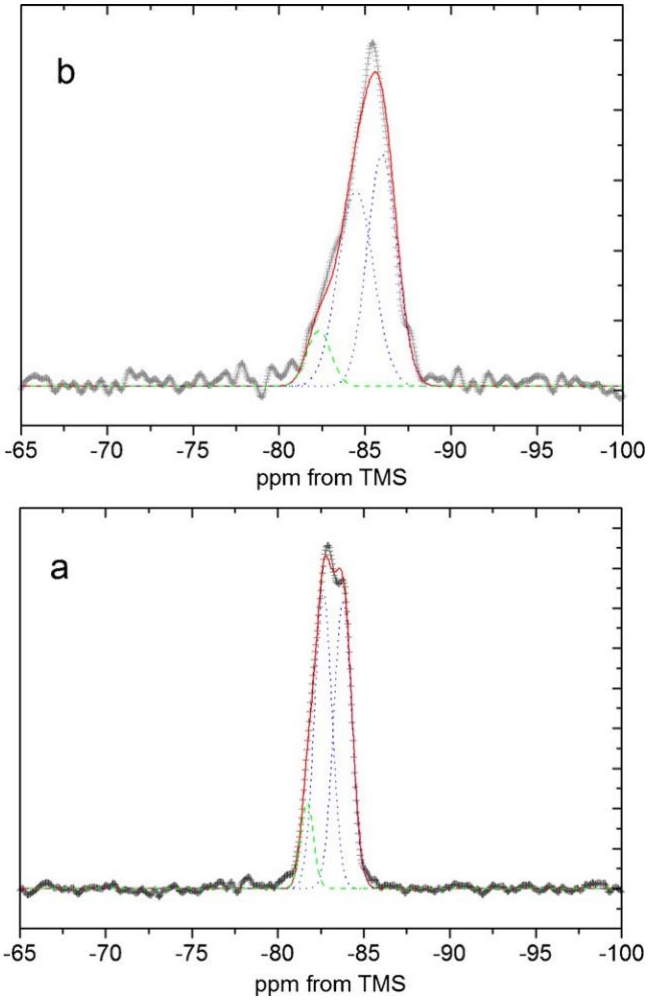

Figure 5: Experimental (crosses) and calculated (solid line) ^{29}Si MAS NMR spectra of *a)* $La_{1.0}Y_{1.0}Si_2O_7$ annealed at 1600 ºC for 2 days and *b)* G-$La_2Si_2O_7$. Individual contributions appear as discontinuous lines.

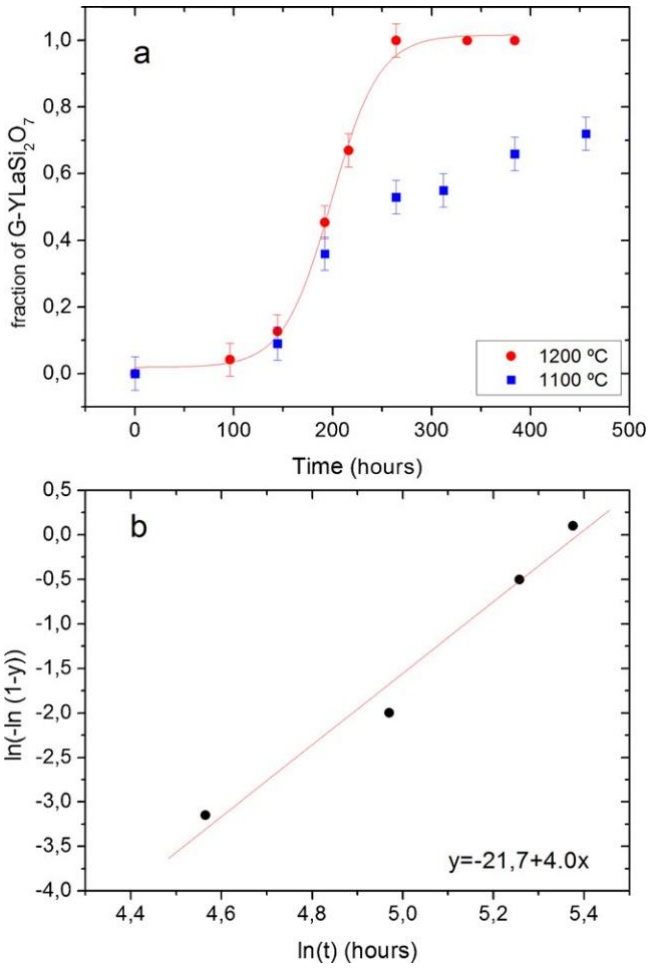

Figure 6: a) Fraction of G-$La_{1.0}Y_{1.0}Si_2O_7$ versus calcination time at 1200 ºC (circles) and 1100 ºC (squares). b) Plot of ln –ln (1-*y*) against ln *t* for the transformation of A-$La_{1.0}Y_{1.0}Si_2O_7$ in G- $La_{1.0}Y_{1.0}Si_2O_7$.

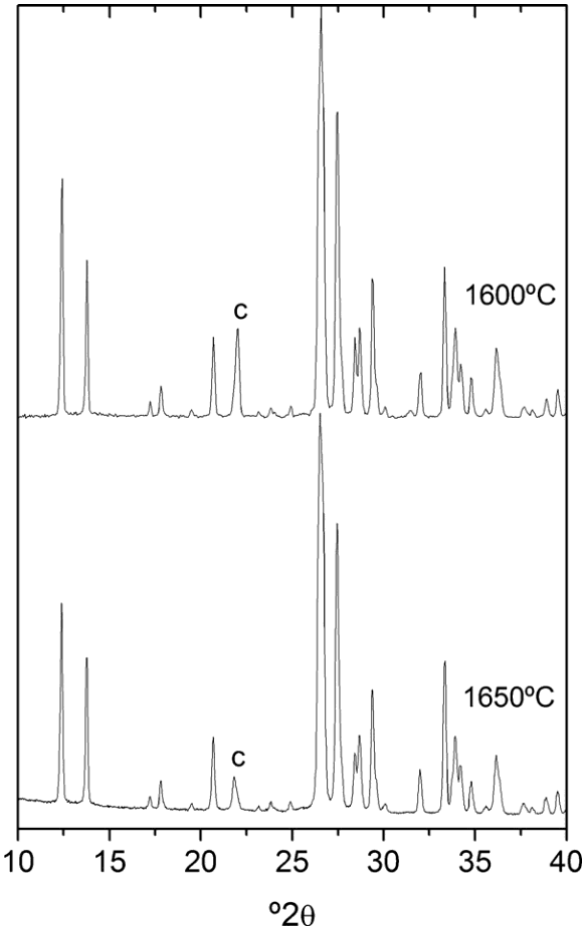

Figure7: XRD patterns (CuKα radiation) of $La_{1.0}Y_{1.0}Si_2O_7$ annealed at *a)* 1600 ºC and *b)* 1650ºC.

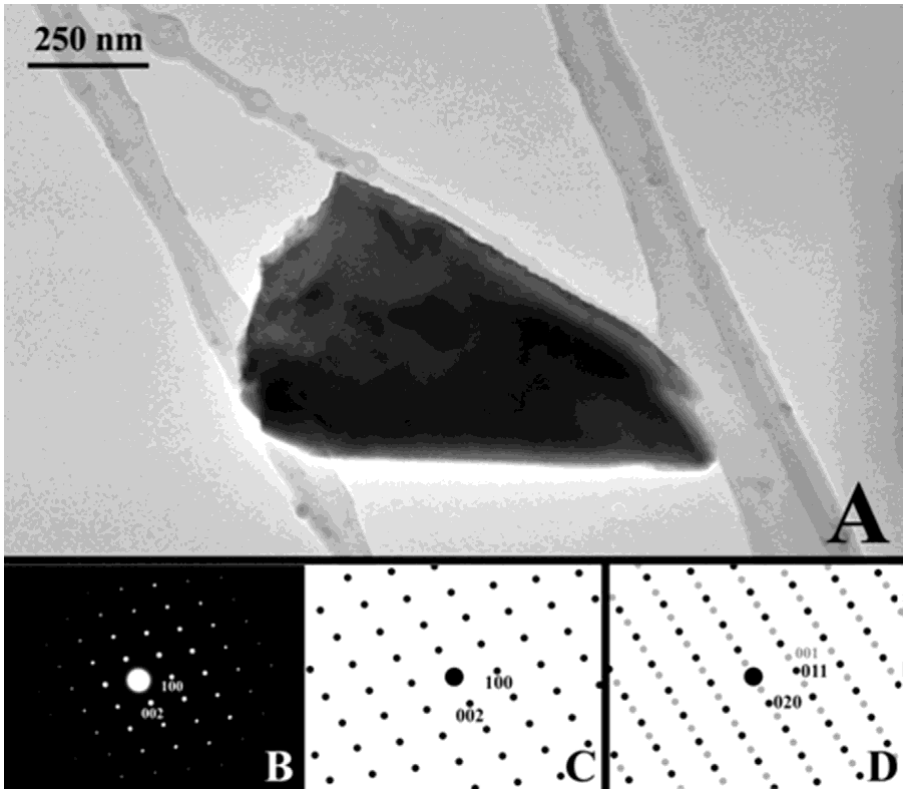

Figure 8: A) Bright field TEM micrograph of a $La_{1.0}Y_{1.0}Si_2O_7$ grain of the sample calcined at 1650ºC. B) Electron diffraction pattern of the grain presented in a. The pattern has been indexed along the [010] of the monoclinic G-$La_{1.0}Y_{1.0}Si_2O_7$ phase. C) Simulation of the electron diffraction pattern along the [010] of the monoclinic G-$La_{1.0}Y_{1.0}Si_2O_7$. D) Simulation of the electron diffraction pattern along the [100] of the possible triclinic F-$La_{1.0}Y_{1.0}Si_2O_7$. Spots in grey correspond to the (001) and (100) family of planes that do not appear on the pattern shown in c.

Table 1
Polymorphs found after calcination of the xerogel with La/Y ratio = 1. A = A-(La,Y)2 Si2 O7 ; G = G-(La,Y)2 Si2 O7 .

Temp (◦C)	1 day	2 days	4 days	6 days	8 days	9 days	11 days
1100			A	A+G	A+G		G+A
1200	A		A+G	A+G	A+G	G+A	G
1250			G				
1300		G	G				
1500		G	G				
1600		G					

Table 2
Refined atomic coordinates for G-La1.0 Y1.0 Si2 O7 from synchrotron X-ray powder diffraction data collected at RT. Space group P21 /c. a = 5.38156(1) A˚ ; b = 8.60239(2) A˚ ; c = 14.0321(1) A˚ and β = 113.212(1)◦.

Atom	x	y	z	Uiso	Occ
La1/Y1	0.52741(7)	0.80418(3)	0.77121(2)	0.00650(8)	0.8530(15)/0.1470(15)
La2/Y2	0.85825(8)	0.60690(4)	0.59019(3)	0.00544(11)	0.1470(15)/0.8530(15)
Si1	0.7955(3)	0.24644(13)	0.02173(10)	0.0054(3)	1
Si2	0.9102(3)	0.50152(15)	0.18201(9)	0.0061(3)	1
O1	0.8513(6)	0.4215(3)	0.0711(2)	0.0152(9)	1
O2	0.0675(6)	0.1329(3)	0.0749(2)	0.0046(7)	1
O3	0.5570(6)	0.1614(3)	0.0447(2)	0.0098(8)	1
O4	0.7618(5)	0.2547(3)	0.90629(19)	0.0044(7)	1
O5	0.7413(5)	0.4251(3)	0.2419(2)	0.0025(7)	1
O6	0.2244(6)	0.4800(3)	0.2577(2)	0.0075(7)	1
O7	0.8118(5)	0.6824(3)	0.17066(19)	0.0056(7)	1

Table 3
29 Si MAS NMR parameters obtained from simulation of the spectra of La1.0 Y1.0 Si2 O7 and La2 Si2 O7 calcined at 1600 ◦C for 2 days.

Peak	Chemical shift (ppm)	FWHM (ppm)	Area under the curve (%)	Assignation
La1.0 Y1.0 Si2				
1	−86.0	2.1	45	G-La1.0 Y1.0 Si2 O7
2	−84.5	2.4	46	G-La1.0 Y1.0 Si2 O7
3	−82.3	1.6	9	o-La1.0 Y1.0 Si2 O7
La2 Si2 O7				
1	−83.8	1.2	45	G-La2 Si2 O7
2	−82.7	1.2	46	G-La2 Si2 O7
3	−81.7	0.9	9	Si in another phase